

# Proton radiation damage in high-resistivity n-type silicon CCDs

C. J. Bebek, D. E. Groom, S. E. Holland, A. Karcher, W. F. Kolbe, J. Lee, M. E. Levi, N. P. Palaio,  
B. T. Turko, M. C. Uslenghi, M. T. Wagner, G. Wang  
E.O. Lawrence Berkeley National Laboratory, Berkeley, CA 94720

## ABSTRACT

A new type of p-channel CCD constructed on high-resistivity n-type silicon was exposed to 12 MeV protons at doses up to  $1 \times 10^{11}$  protons/cm<sup>2</sup>. The charge transfer efficiency was measured as a function of radiation dose and temperature. We previously reported that these CCDs are significantly more tolerant to radiation damage than conventional n-channel devices. In the work reported here, we used pocket pumping techniques and charge transfer efficiency measurements to determine the identity and concentrations of radiation induced traps present in the damaged devices.

**Keywords:** CCD, Radiation Damage, High Resistivity Silicon, Charge Transfer Efficiency

## 1. INTRODUCTION

A new type of CCD has been developed at Lawrence Berkeley National Laboratory (LBNL) using high-resistivity n-type silicon with boron implants to create p-channel devices [1]. Unlike conventional CCDs fabricated on low-resistivity p-type silicon that can be depleted only over distances of a few microns [2], these devices can be fully depleted over their entire 300  $\mu\text{m}$  wafer thickness. As a result they can be operated backside illuminated to achieve improved blue response without the need of the thinning process step required with ordinary CCDs. In addition, the large thickness of their depletion region increases the absorption of near infrared photons resulting in a significantly enhanced red response. Experience with the use of high-resistivity n-type silicon in the manufacture of radiation detectors for high energy physics experiments suggests that CCDs fabricated using this material should be resistant to radiation.

Proton irradiation is known to produce displacement damage in silicon that leads to the formation of trapping sites in the material. In our p-channel CCDs, hole traps in the channel region of the CCD with energies close to the valence band edge can capture charge during readout and degrade the charge transfer efficiency (CTE). In addition the presence of midband traps in the depletion region can lead to an increase in dark current.

Conventional CCDs employ a phosphorus-doped channel and are susceptible to the generation in a radiation environment of phosphorus vacancy (PV) electron traps that degrade the CTE [3]. In p-channel devices the dominant hole trap after irradiation is expected to be the divacancy (VV) [4,5]. Divacancy formation in p-channel CCDs is generally considered to be less favorable than PV formation in n-channel devices. In addition the VV trap energy (0.20 eV above the valence band) lies further from the middle of the band gap than the PV trap (0.45 eV below the conduction band) and should therefore contribute less to dark current [3,4]. The LBNL CCDs also incorporate "notch" implants [6] in the serial channel that decrease the available volume for small charge packets further reducing the contribution of the hole traps to the readout CTE.

## 2. MODEL OF THE TRAP EFFECTIVENESS AND CTE

The CTE is one of the most critical CCD parameters influenced by radiation. As the charge  $Q_{\text{col}}$  collected in each pixel is clocked through the device a fraction is lost due to capture by traps located in the serial and parallel channels. The fractional amount successfully transferred in each transition is defined as the CTE. The amount of charge reaching the readout transistor after  $n$  shifts is given by  $Q_{\text{out}} = Q_{\text{col}} \times \text{CTE}^n$ . In general, the CTE is a function of the temperature,

readout speed, signal size, background charge and clocking waveform. For example, the clocking parameters for vertical and horizontal data transfer are quite different in our measurements and we measure them separately into the components  $CTE_{\text{serial}}$  and  $CTE_{\text{parallel}}$ .

A number of authors have described [2] the contribution of traps to the charge transfer inefficiency ( $CTI = 1 - CTE$ ) based on the Shockley-Hall-Reed theory. Each trap is characterized by its trapping cross section  $\sigma$  and its trapping state energy  $E_t$  below the conduction band (for electron traps) and above the valence band (for hole traps). These trap characteristics allow us to calculate the capture time  $\tau_c$  and emission time  $\tau_e$  time constants for the trap

$$\tau_e = \frac{e^{E_t / kT}}{\sigma v_{th} N_c} \quad (1)$$

$$\tau_c = \frac{1}{\sigma v_{th} n_e} \quad (2)$$

where  $v_{th}$  is the thermal velocity of the carriers,  $n_e$  is density of carriers (electrons or holes), and  $N_c$  is the effective density of states. According to a simplified model [4,7] in which the trap capture time is considered to be instantaneous it can be shown that the CTI is given by

$$CTI = \frac{N_t}{n_e} F = \frac{N_t}{n_e} e^{-\frac{T_0}{\tau_e}} \left[ 1 - e^{-\frac{(-2T_0 + N_z T_p)}{\tau_e}} \right] \quad (3)$$

where  $N_t$  is the trap density and  $n_e$  is the electron (hole) density in a pixel holding a charge packet to be transferred. This pixel is then followed by  $N_z$  empty pixels before the next charged pixel is encountered.  $T_0$  is the overlap between clocks and  $T_p$  is the clock period. The equation is derived for the symmetrical case where  $T_p = 3T_0$ . In Eq. 3 the fractional charge transfer loss (CTI) is given by the ratio of the number of traps to the number of electrons in the pixel multiplied by an exponential “trap effectiveness factor”  $F$ .  $F$  is the probability that a filled trap releases its charge during the overlap period,  $T_0$ , times the probability that a trap filled by a previous event is still filled. It is this factor that determines the range of temperatures over which the trap is effective for a given clocking rate. We have extended this theory to account for finite  $\tau_c$  and a more generic clocking scheme with results shown in the appendix.

## 2. EXPERIMENT

In this study a set of 4 CCDs was characterized and then irradiated at the LBNL 88-inch Cyclotron. A proton energy of 12 MeV was chosen to provide both a high Non Ionizing Energy Loss (NIEL) and a reasonable penetration depth to generate a uniform damage profile over the device thickness. The dose can readily be scaled to other energies using, for example, the NIST PSTAR data [8].

The CCDs are 512x1024 pixel, 15  $\mu\text{m}$  pitch, engineering grade devices and were not backside processed. They are 600  $\mu\text{m}$  thick and cannot be operated fully depleted. Accordingly, they were used as front-illuminated devices. Otherwise they were fully functional and exhibited excellent pre-radiation CTE, read noise, and dark current. The four CCDs were irradiated to total doses of  $5 \times 10^9$ ,  $1 \times 10^{10}$ ,  $5 \times 10^{10}$ , and  $1 \times 10^{11}$  protons/cm<sup>2</sup>. The irradiation was performed at a dose rate of less than  $2 \times 10^7$  protons/cm<sup>2</sup>/s with the devices operated unpowered at room temperature.

For characterization, the CCDs were mounted in a LN2 dewar fabricated in-house and provided with temperature control capabilities from 90 to 220 K. Measurements were performed using a commercial CCD controller modified to provide the voltages necessary to operate the p-channel devices.

### 3. CHARGE TRANSFER EFFICIENCY

The CTE is measured by exposing the CCD to a  $^{55}\text{Fe}$  x-ray source that deposits on average  $1620 e^-$ . The source was mounted inside the dewar on a control arm which provided an adjustable exposure time set to deposit one x-ray about every 50-70 pixels. To measure the CTE, serial and parallel stacking plots are generated from the x-ray image by collapsing all the data on the vertical and horizontal axes respectively. The serial and parallel CTE components can then be determined by fitting the cluster of single pixel x-ray events to the CTE equation. Figure 1 shows a typical stacking plot for the parallel CTE calculation.

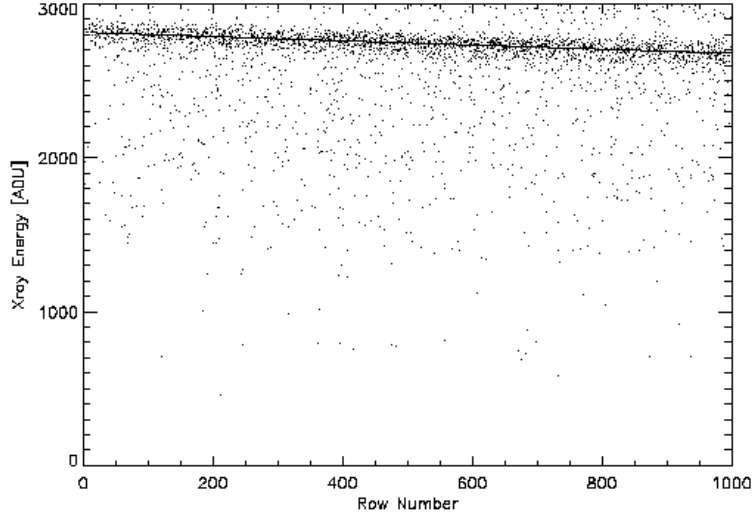


Fig.1: X-ray stacking plot for parallel CTE calculation at a proton dose of  $1 \times 10^{10}$  protons/cm<sup>2</sup> measured at 128 K. The single pixel x-ray events cluster along a line whose slope provides a measure of the CTE.

The CTE was measured as a function of temperature for each of the irradiated devices. These measurements and a determination of the dark current have been reported elsewhere [9]. Figure 2 shows the CTE as a function of proton dose for a temperature of 128 K, close to the optimal value for the readout speed of 30 kpixel/sec used. The error bars shown represent the statistical uncertainty only in the width of the x-ray lines in the corresponding stacking plots used in the CTE calculation. Before irradiation all CCDs showed a CTE greater than 0.999999. Since the measurements were made using different CCDs irradiated at the same time, we cannot separate out possible device-to-device variations from the results although all the CCDs behaved nearly identically prior to irradiation. As discussed in the earlier paper [9], the observed CTE degradation as a function of dose when converted to MeV/g is more than an order of magnitude smaller than that found for typical n-channel CCDs.

The temperature dependence of the serial and parallel CTE for the irradiated devices is shown in Fig. 3 for the highest dose of  $1 \times 10^{11}$  protons/cm<sup>2</sup>. The difference between the serial and parallel CTE results is striking and is a result of the different clocking speeds used. In both cases the inefficiency of the radiation induced traps at high temperatures, where the clock overlap times are longer than the detrapping time, can be seen. At low temperatures, in the serial case, the detrapping time becomes longer than the time between individual x-rays and the traps remain saturated and therefore ineffective. Because of the much slower parallel clocking used, this does not happen for the parallel CTE case.

### 4. IDENTIFYING TRAPS WITH POCKET PUMPING

It is clear from Fig. 3 that the observed CTE behavior is strongly affected by the nature of the radiation induced traps and the details of the clocking used to read out the CCD. It is important, therefore, to identify the traps involved and determine their characteristics. We use the pocket pumping procedure to investigate trap behavior. A detailed

knowledge of the traps involved will enable us not only to best establish appropriate operating conditions for our CCDs but also, hopefully, to determine better material and fabrication protocols which will lead to even more radiation resistant devices.

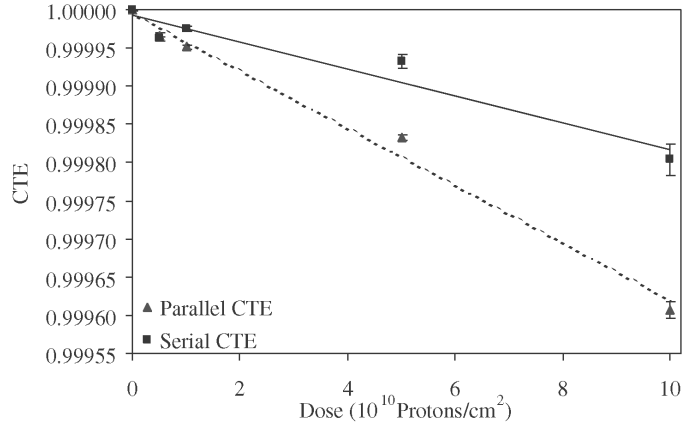


Fig. 2: CTE degradation as a function of proton dose measured at 128 K.

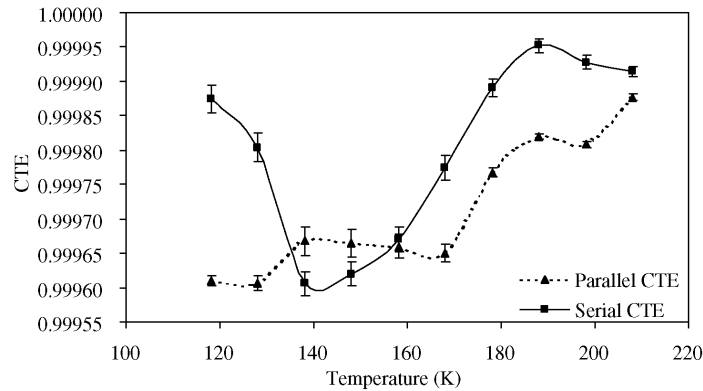


Fig. 3: CTE as a function of temperature for dose of  $1 \times 10^{11}$  protons/cm<sup>2</sup>.

#### 4.1. The Pocket Pumping Method

In the pocket pumping method [2], one first illuminates the CCD with a low intensity light source to provide a flat field level, then shifts the accumulated charge back and forth a number of pixels in the parallel direction. After doing this repeatedly for a determined number of cycles, the CCD is read out in the normal manner. If the CCD is perfect, *i.e.*, contains no traps, one will get an image essentially identical to one obtained without the cycling. If there are traps they will initially be filled by the flat field illumination. But as the charge is cycled back and forth past the individual traps they will retain, release, or retrap the charge according to their lifetime and the pumping rates. Two different kinds of traps, forward and reverse, can be defined according to whether their charge is left behind on the upward or downward portion of the cycle. After many cycles there will be a peak produced by the accumulated charges and a corresponding valley from which they are drawn.

Figure 4 shows example pocket pumping images produced by 60000 cycles of a 5-pixel shift. In each case the traps can be seen as peaks (bright points) with adjacent valleys (dark lines). The measured density of traps in the un-irradiated CCD at left was 0.0021 traps/pixel while that measured for the CCD at right that received a dose of  $1 \times 10^{10}$  protons/cm<sup>2</sup>

was 0.096 traps/pixel. The magnified inserts show the traps in greater detail. In them can be seen the forward and reverse traps in which the dark valleys extend in opposite directions from the bright peaks.

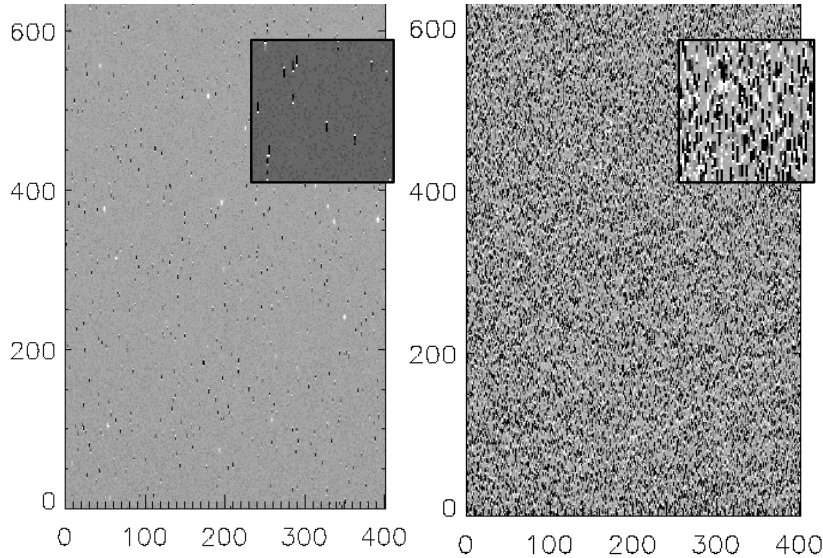


Fig. 4: Pocket pumping image for two cases: at left an un-irradiated CCD and at right a CCD dosed to  $1 \times 10^{10}$  protons/cm<sup>2</sup>.

The effectiveness of a trap at a particular temperature and pumping rate, also called the trap depth, can be measured by determining the height of the peak produced by a given number of pumping cycles. In fact it can be defined as the peak height per cycle. A histogram of a one-shift pocket pumped image shown in Fig. 5 reveals the amplitude of the pumping peak, the depletion peak, a saturated peak, and the primary flat field level of the image. The amplitude of the pocket pumping peak is measured from the flat field level and converted to electrons (holes) by an independent measurement of the CCD gain using the <sup>55</sup>Fe x-ray source.

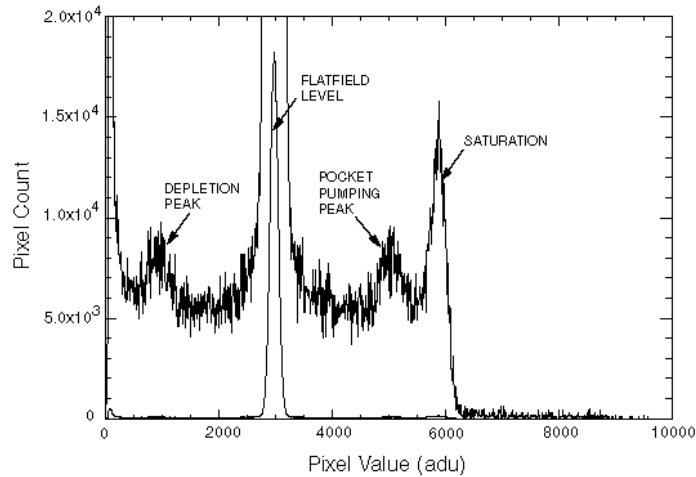


Fig. 5: Histogram showing the pocket pumping peak, the corresponding depletion peak, a saturation peak and the flat field level.

## 4.2. Measurement of Trap Effectiveness

The above technique was used to measure the trap effectiveness (trap depth) as a function of temperature for each of the CCDs. In these measurements either 1 or 5 shifts per cycle were used together with a clock overlap of 19.5  $\mu$ s. The peak was identified from the histogram as in the above example for at least two different cycle counts and normalized to the CCD gain. Figure 6 shows the measured trap effectiveness (closed circles) obtained one day after irradiation for a dose of  $1 \times 10^{10}$  protons/cm<sup>2</sup> together with calculated effectiveness curves for several candidate traps as discussed below. The figure shows not one but two peaks, one centered at about 160 K and the other at 190 K. Careful repeated measurements the CCDs at different times up to about 60 days after the initial irradiation showed the both peaks could be detected in all cases. The upper peak however became increasingly weaker (in the histogram) and very difficult to detect as time progressed indicating decay in its concentration.

It is also possible to identify the subset of traps contributing to each of these two peaks. To do this a trap “map” is generated at a temperature near one of the peaks but far enough away from the other to exclude its activity as much as possible. This map is then used as a filter in the histogram calculation, including only points detected as peaks in the map. When this is done, only one of the two peaks is seen at a time proving that each of the two peaks arises from a different set of traps.

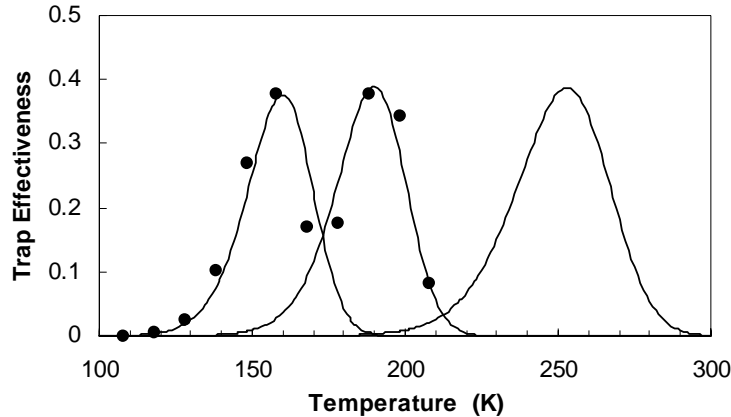


Fig. 6: Measured trap depth (closed circles) together with computed trap effectiveness for 3 hole traps: divacancy with peak at 160 K, carbon interstitial at 190 K, and carbon-oxygen at 253 K.

## 4.3. Hole Traps in n-type Silicon

Because of their use in high energy physics experiments, radiation damage in silicon particle detectors has been studied extensively. Moll [10] has summarized much of the available material on radiation induced traps in n-type silicon and extended it by Deep Level Transient Spectroscopy (DLTS) measurements. Table 1 shows the parameters for a number of traps of interest. In the table, the capture cross sections were determined with temperature independent density-of-states effective valence band mass ( $m^* = 0.549m_0$ ) as given in [11].

As a result of the fabrication process, carbon and oxygen are common impurities in high-resistivity n-type silicon. The radiation induced interstitial carbon trap  $C_i$  is most likely produced via the following mechanism: proton collisions create an interstitial Si atom which then replaces a substitutional carbon ( $C_s$ ) in the lattice. The resulting  $C_i$  is not stable but decays eventually to a  $C_iO_i$  or a  $C_iC_s$  trap. The decay rate at room temperature was found to depend strongly on the C and O concentrations but generally required a few days [10]. The  $C_iC_s$  hole trap has a very low energy ( $\sim 0.08$  eV) and should not contribute to the CTE over our temperature range. The  $C_iO_i$  trap, however, is a candidate for CTE degradation.

Vacancies produced by proton irradiation migrate around the lattice until they form pairs with other impurities or with other vacancies. Most stable of these are the amphoteric (hole or electron) divacancy VV and the VO electron trap. The VV trap is considered to be the dominant hole trap expected in irradiated p-channel CCDs [4,5].

Trap Name	Cross Section [cm <sup>2</sup> ]	Energy Level [eV]
VV <sup>(+/0)</sup>	8.0x10 <sup>-16</sup>	0.200
C <sub>i</sub> <sup>(+/0)</sup>	4.28x10 <sup>-15</sup>	0.284
C <sub>i</sub> O <sub>i</sub> <sup>(+/0)</sup>	2.45x10 <sup>-15</sup>	0.360

Table 1: Some hole traps produced by proton irradiation

#### 4.4. Trap Effectiveness

According to the model presented above (Eq. 3) the trap effectiveness factor F gives the temperature range over which a given trap is effective in reducing the CTI. This is the same quantity that is measured in the pocket pumping experiments. In that case the clock overlap time was  $T_0 = 19.5 \times 10^{-6}$  sec and the clocking was symmetrical with  $T_p = 3T_0$ . Using the trap parameters from Table 1 and the improved equations given in the appendix with the above timing we computed the trap effectiveness factors for each trap. The results are shown in Fig. 6 together with the measured pocket pumping data.

If we compare the positions of the two calculated peaks for the divacancy and the carbon interstitial with the measured peak positions of the pocket pumping data we find excellent agreement thereby confirming the presence of these two traps. The third peak shown in Fig. 6 is not experimentally accessible to the pocket pumping study because the dark current is too large at the high temperatures required to measure it. However, as shown below we believe it to be present and a significant contributor to the radiation degraded CTE.

## 5. FITTING CTE DATA TO TRAP DENSITIES

The pocket pumping experiments served to identify the divacancy and the carbon interstitial as two radiation induced traps that were candidates for impacting the CTE of the irradiated devices. In addition it was observed that the carbon interstitial trap was becoming increasingly harder to observe as time elapsed after the radiation dose. This suggested that the concentration of this trap was decaying with time. We then attempted to fit the <sup>55</sup>Fe CTE data obtained at different doses and delay times after irradiation to the theoretical CTE using these two traps as the source of the CTE degradation. The enhanced  $CTI = 1 - CTE$  equation given in the appendix was used in the fits. When this was done we found that we could not get very good fits until we added the third trap, the C<sub>i</sub>O<sub>i</sub> trap, to the fit. The resulting fits are illustrated below in Fig. 8 for doses of  $1 \times 10^{11}$  protons/cm<sup>2</sup> (measured after 9 days) and  $5 \times 10^{10}$  protons/cm<sup>2</sup> (measured after 13 days).

The fit parameters given in Table 2 show the concentrations of each of the three traps included in the fit. The serial and parallel CTI data were fit simultaneously for each of the two cases. The serial register of our CCD contains a notch implant that reduces the effective volume and hence exposure to traps for small charge levels. This notch was not present in the parallel register of the devices tested here. To account for this, we include a compensating factor adjusted to 1.6 ( $N_i$  in appendix). As can be seen from the fit results, the concentration of the carbon interstitial trap C<sub>i</sub>, is found to be essentially zero within the statistical uncertainty in both cases. To find convincing evidence of a CTE contribution from the C traps would require measurements at earlier times than we were able to achieve in this study.

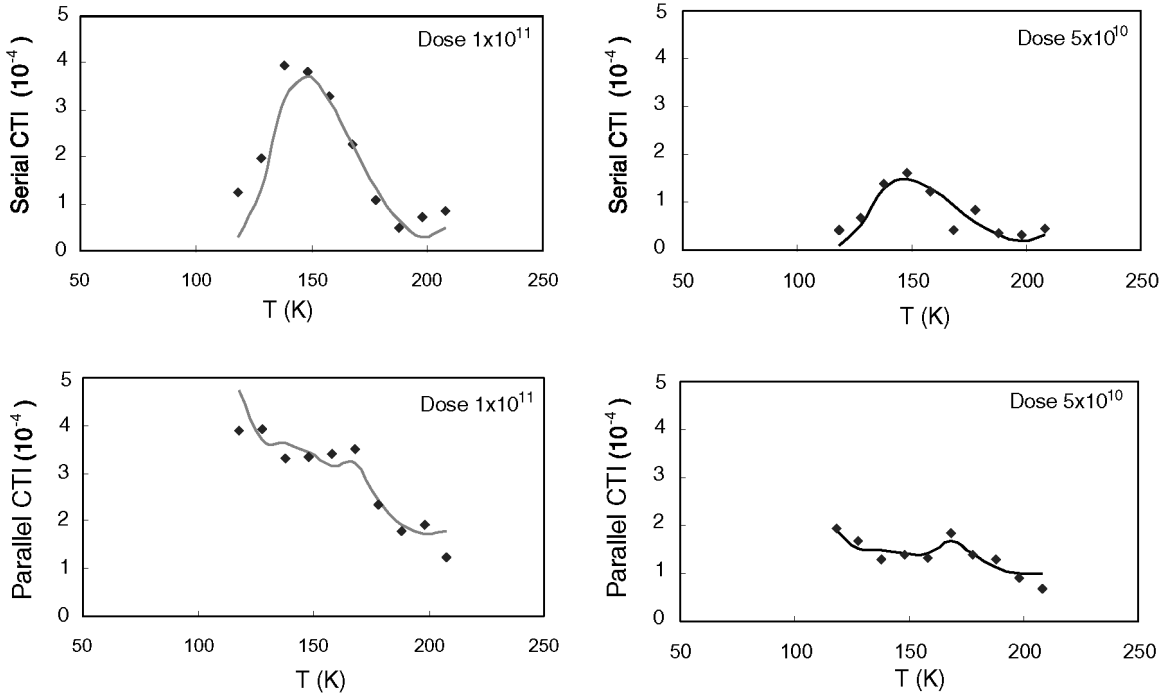


Fig. 7: Representative fits of the measured CTI of two CCDs which received doses of  $1 \times 10^{11}$  protons/cm<sup>2</sup> and  $5 \times 10^{10}$  protons/cm<sup>2</sup> respectively measured 9 and 13 days after exposure.

Dose (p/cm <sup>2</sup> )	Time	Trap concentration (pixel <sup>-1</sup> )		
		V-V	C	C-O
$1 \times 10^{11}$	9 days	$0.680 \pm 0.045$	$-0.079 \pm 0.040$	$0.283 \pm 0.032$
$5 \times 10^{10}$	13 days	$0.268 \pm 0.020$	$-0.024 \pm 0.018$	$0.156 \pm 0.015$

Table 2: Trap concentrations 9 days and 52 days after irradiation extracted from simultaneously fitting the parallel and serial CTIs for the  $1 \times 10^{11}$  proton/cm<sup>2</sup> dosed device.

Figure 8 shows the fitted trap density results obtained for each of the four irradiation doses. Because of delays (ranging over a 50 day period) in measuring the CCDs after irradiation, some of the data was obtained at later times than others. Hence any parameter variations due to growth/decay of the various traps are not accounted for. Error brackets in Fig. 8 account for the statistical accuracy of the fits but do not include errors in the fits of the CTE data itself. We included all three of the traps in our analysis but found the contributions of the C trap to be equal to zero within 2 standard deviations in all measurements.



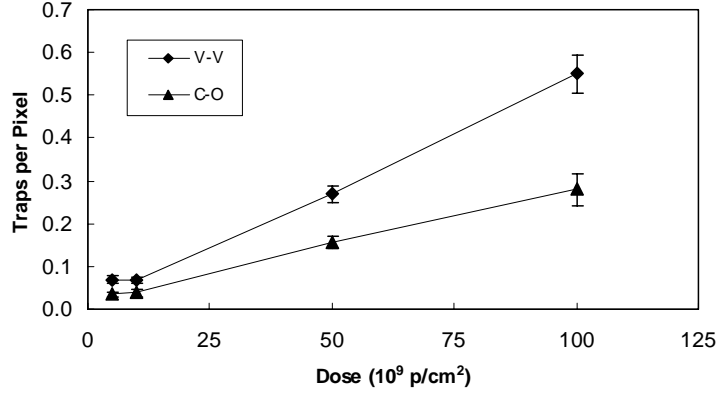


Fig. 8: Dose dependence of the fitted trap densities VV (top), CO (below).

## 6. SUMMARY

Four LBNL p-channel CCDs were irradiated with protons at 12 MeV with doses up to  $1 \times 10^{11}$  protons/cm<sup>2</sup>. CTE measurements were performed showing the devices to be significantly more radiation resistant than “standard” n-channel CCDs. Pocket pumping experiments were performed on the CCDs that enabled us to identify the primary trapping centers impacting the CTE. The CTE data was fit to an improved model appropriate to our non-symmetrical clocking using three traps identified in the pocket pumping analysis. The resulting fits were in reasonable agreement with the accumulated doses. They confirmed the importance of the divacancy and the carbon-oxygen traps in degrading the CTE of the CCDs. Additional measurements are planned to more precisely determine the concentrations of the stable traps at a future date. The information gained in these experiments will enable us to better predict long term device performance in the radiation environment and to tune the fabrication and wafer materials selection processes to make even more proton resistant CCDs.

## 7. APPENDIX

Equation 3 in the text is valid for a symmetrical clocking sequence in which the clock overlaps are 1/3 of the clock period. Often, as in our case the clock periods for each of the three phases are not equal. Figure 9 below shows our serial clocking sequence. A similar pattern applies to the parallel clock sequence we use. In addition, we include in the derivation additional terms accounting for a finite trapping time,  $\tau_c$ . We define  $T_0$  as the clock overlap,  $T_p$  as the clock period, and  $T_1 = T_p - 6T_0$ . Then, using Eq. 1 and 2 for  $\tau_e$  and  $\tau_c$  we obtain for the CTI

$$\text{CTI}(T) := \sum_i N_i \cdot M(n, T, E_i, \sigma_i) \cdot (F_{g1}(T, E_i, \sigma_i) + F_{g2}(T, E_i, \sigma_i) + F_{g3}(T, E_i, \sigma_i))$$

where the summation is over the densities,  $N_i$  of the traps of energy  $E_i$  and cross section  $\sigma_i$  present.  $M$  and the  $F_g$  terms for each of the three phases are given below

$$M(n, T, E, \sigma) := \frac{1}{3 \cdot n} \cdot \frac{\tau_e(T, E, \sigma)}{\tau_e(T, E, \sigma) + \tau_c(T, n, \sigma)}$$

$$F_{g1}(T, E, \sigma) := \left[ \begin{array}{cc} \frac{-T_0}{0.5e^{\frac{-T_0}{\tau_e(T, E, \sigma)}} + (1-0.5)e^{\frac{-2 \cdot T_0}{\tau_e(T, E, \sigma)}}} & \frac{-2 \cdot T_0}{\tau_e(T, E, \sigma)} \end{array} \right] \left[ \begin{array}{c} \frac{T_1 + 3 \cdot T_0 - N_z \cdot (T_1 + 6 \cdot T_0)}{\tau_e(T, E, \sigma)} \\ 1 - e \end{array} \right] \left[ \begin{array}{c} \frac{-(T_1 + 3 \cdot T_0) \cdot (\tau_e(T, E, \sigma) + \tau_c(T, n, \sigma))}{\tau_e(T, E, \sigma) \cdot \tau_c(T, n, \sigma)} \\ 1 - e \end{array} \right]$$

$$F_{g2}(T, E, \sigma) := \left[ \begin{array}{cc} \frac{-T_0}{0.5e^{\frac{-T_0}{\tau_e(T, E, \sigma)}} + (1-0.5)e^{\frac{-(2 \cdot T_0)}{\tau_e(T, E, \sigma)}}} & \frac{-(2 \cdot T_0)}{\tau_e(T, E, \sigma)} \end{array} \right] \left[ \begin{array}{c} \frac{3 \cdot T_0 - N_z \cdot (T_1 + 6 \cdot T_0)}{\tau_e(T, E, \sigma)} \\ 1 - e \end{array} \right] \left[ \begin{array}{c} \frac{-(3 \cdot T_0) \cdot (\tau_e(T, E, \sigma) + \tau_c(T, n, \sigma))}{\tau_e(T, E, \sigma) \cdot \tau_c(T, n, \sigma)} \\ 1 - e \end{array} \right]$$

$$F_{g3}(T, E, \sigma) := \left[ \begin{array}{cc} \frac{-(T_0 + T_1)}{0.5e^{\frac{-(T_0 + T_1)}{\tau_e(T, E, \sigma)}} + (1-0.5)e^{\frac{-(2 \cdot T_0 + T_1)}{\tau_e(T, E, \sigma)}}} & \frac{-(2 \cdot T_0 + T_1)}{\tau_e(T, E, \sigma)} \end{array} \right] \left[ \begin{array}{c} \frac{3 \cdot T_0 - N_z \cdot (T_1 + 6 \cdot T_0)}{\tau_e(T, E, \sigma)} \\ 1 - e \end{array} \right] \left[ \begin{array}{c} \frac{-(3 \cdot T_0) \cdot (\tau_e(T, E, \sigma) + \tau_c(T, n, \sigma))}{\tau_e(T, E, \sigma) \cdot \tau_c(T, n, \sigma)} \\ 1 - e \end{array} \right]$$

The measured CTI data was then fit to these equations using the clocking parameters  $T_0$  and  $T_1$  used in the experiment. In the present case  $T_0 = 20 \mu\text{s}$  and  $T_1 = 25.9 \text{ ms}$  for parallel clocking and  $T_0 = 2.0 \mu\text{s}$  and  $T_1 = 20.4 \mu\text{s}$  for serial clocking.

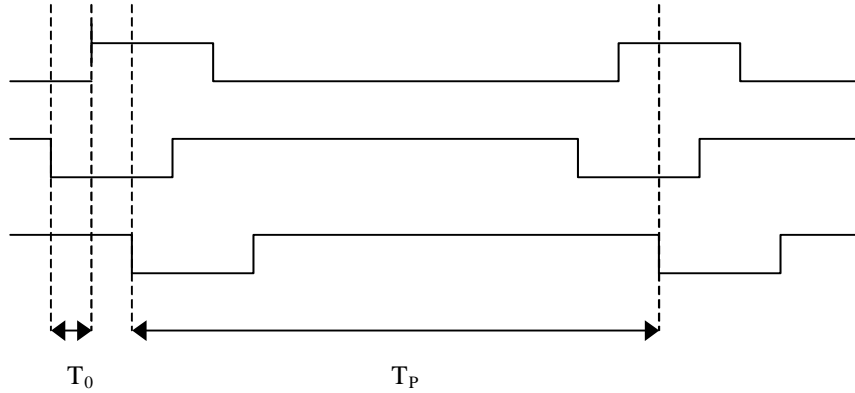


Fig. 9: Typical asymmetrical three phase clocking sequence used in CCD readout.

## ACKNOWLEDGEMENTS

This work was supported by DOE contract No. DE-AC03-76SF00098, NSF/ATI, NASA/SADD, and under contract to the USAF.

## REFERENCES

1. S.E. Holland et al., "A 200x200 pixel CCD image sensor fabricated on high-resistivity silicon," IEDM Technical Digest, pp. 911-914, 1996.
2. J. Janesick, "Scientific Charge-Coupled Devices," SPIE Press, 2001.
3. J. Janesick, G. Soli, T. Elliot, and S. Collins, "The effects of proton damage on charge-coupled devices," *Charge-Coupled Devices and Solid State optical Sensors II*, Proc. of SPIE, 1447, pp. 87-108, 1991.
4. J.P. Spratt, B.C. Passenheim, R.E Leadon, "The effects of nuclear radiation on p-channel CCD imagers," in 1997 IEEE Radiation Effects Data Workshop, NSREC Snowmass 1997. Workshop Record. Held in conjunction with IEEE Nuclear and Space Radiation Effects Conference.
5. G.R. Hopkinson, "Proton Damage Effects on P-channel CCDs," IEEE Trans. Nucl. Sci., 46(6), pp. 1790-1796, 1999.
6. R.A. Bredthauer, J.H. Pinter, J.R. Janesick, and L.B. Robinson, "Notch and large area CCD imagers," *Charge-Coupled Devices and Solid State optical Sensors II*, Proc. of SPIE, 1447, pp. 310-315, 1991.
7. A.M. Mohsen and M.F. Tompsett, "The effects of bulk traps on the performance of bulk channel charge-coupled devices," IEEE Trans. Elec. Devices, ED-21(11), pp. 701-712, 1974.
8. <http://physics.nist.gov/PhysRefData/Star/Text/contents.html> NIST: PSTAR data.
9. C. Bebek, *et al.*, "Proton Radiation Damage in P-Channel CCDs Fabricated on High-Resistivity Silicon," *IEEE Nuclear Sci. Symposium Proceedings*, San Diego, CA, Nov. 2001.
10. M. Moll, "Radiation Damage in Silicon Particle Detectors," PhD dissertation, Physics Dept., Univ. of Hamburg, Germany, 1999.
11. S.M. Sze. *Physics of Semiconductor Devices*. John Wiley & Sons, 2<sup>nd</sup> edition, 1981.